



1 **Reconstruction of global surface ocean $p\text{CO}_2$ using**
2 **region-specific predictors based on a stepwise FFNN**
3 **regression algorithm**

4 Guorong Zhong^{1,2,3,4}, Xuegang Li^{1,2,3,4*}, Jinming Song^{1,2,3,4*}, Baoxiao Qu^{1,3,4}, Fan
5 Wang^{1,2,3,4}, Yanjun Wang^{1,4}, Bin Zhang^{1,4}, Xiaoxia Sun^{1,2,3,4}, Wuchang Zhang^{1,3,4},
6 Zhenyan Wang^{1,3,4}, Jun Ma^{1,3,4}, Huamao Yuan^{1,2,3,4}, Liqin Duan^{1,2,3,4}

7 ¹Institute of Oceanology, Chinese Academy of Sciences, Qingdao 266071, China

8 ²University of Chinese Academy of Sciences, Beijing 101407, China

9 ³Pilot National Laboratory for Marine Science and Technology, Qingdao 266237, China

10 ⁴Center for Ocean Mega-Science, Chinese Academy of Sciences, Qingdao 266071,
11 China

12 *Correspondence to:* Xuegang Li (lixuegang@qdio.ac.cn); Jinming Song
13 (jmsong@qdio.ac.cn)

14 **Abstract:** Various machine learning methods were attempted in the global mapping of
15 surface ocean partial pressure of CO_2 ($p\text{CO}_2$) to reduce the uncertainty of global ocean
16 CO_2 sink estimate due to undersampling of $p\text{CO}_2$. In previous researches the predictors
17 of $p\text{CO}_2$ were usually selected empirically based on theoretic drivers of surface ocean
18 $p\text{CO}_2$ and same combination of predictors were applied in all areas unless lack of
19 coverage. However, the differences between the drivers of surface ocean $p\text{CO}_2$ in
20 different regions were not considered. In this work, we combined the stepwise
21 regression algorithm and a Feed Forward Neural Network (FFNN) to selected
22 predictors of $p\text{CO}_2$ based on mean absolute error in each of the 11 biogeochemical
23 provinces defined by Self-Organizing Map (SOM) method. Based on the predictors
24 selected, a monthly global $1^\circ \times 1^\circ$ surface ocean $p\text{CO}_2$ product from January 1992 to
25 August 2019 was constructed. Validation of different combination of predictors based
26 on the SOCAT dataset version 2020 and independent observations from time series
27 stations was carried out. The prediction of $p\text{CO}_2$ based on region-specific predictors
28 selected by the stepwise FFNN algorithm were more precise than that based on
29 predictors from previous researches. Applying of a FFNN size improving algorithm in
30 each province decreased the mean absolute error (MAE) of global estimate to 11.32
31 μatm and the root mean square error (RMSE) to 17.99 μatm . The script file of the
32 stepwise FFNN algorithm and $p\text{CO}_2$ product are distributed through the Institute of
33 Oceanology of the Chinese Academy of Sciences Marine Science Data Center (IOCAS;
34 <http://dx.doi.org/10.12157/iocas.2021.0022>, Zhong et al., 2021).



35 **1 Introduction**

36 As a net sink for atmospheric CO₂, global oceans have been thought to have
37 removed about one third of anthropogenic CO₂ since the beginning of the industrial
38 revolution (Sabine et al., 2004; Friedlingstein et al., 2019). However, great differences
39 existed between previous estimates of sea-air CO₂ flux, due to large uncertainty in
40 estimates of surface ocean partial pressure of CO₂ (*p*CO₂) (Regnier et al., 2013;
41 Schuster et al., 2013; Wanninkhof et al., 2013; Ishii et al., 2014). surface ocean *p*CO₂ is
42 an essential parameter to describe the release and uptake for atmospheric CO₂ by the
43 oceans in the data-based method. Greater *p*CO₂ of surface water than that of overlying
44 air indicating that CO₂ released from oceans to the air, and absorption of CO₂ by oceans
45 happened when the *p*CO₂ of surface water was lower than that of air. The ocean in these
46 two scenarios is known as oceanic carbon source and oceanic carbon sink respectively.
47 Sparse and uneven observations of surface ocean *p*CO₂ in time and space severely
48 limited the understanding of interannual variability of oceanic carbon sink, and
49 researches based on different methods were carried out to break this barrier. In earlier
50 studies, traditional unitary and multiple regression methods between surface ocean
51 *p*CO₂ and its drivers was attempted in the mapping of surface ocean *p*CO₂, which were
52 limited in specific regions and sometimes even in specific seasons with a relatively high
53 root mean square error (RMSE) (Sarma et al., 2006; Takahashi et al., 2006; Shadwick
54 et al., 2010; Chen et al., 2011; Marrec et al., 2015). Recent researches on artificial neural
55 networks and other machine learning algorithms, such as feed-forward neural network
56 (FFNN) method (Zeng et al., 2014; Zeng et al., 2015; Moussa et al., 2016; Denvil-
57 Sommer et al., 2019) and self-organization mapping (SOM) method (Friedrich and
58 Oeschlies, 2009; Telszewski et al., 2009; Hales et al., 2012; Nakaoka et al., 2013),
59 significantly reduced the bias in the interpolation based on relationships between
60 surface ocean *p*CO₂ and its drivers. In addition, method such as finding better
61 predictors or combining SOM and other neural networks was also attempt to further
62 decrease the *p*CO₂ predicting error (Hales et al., 2012; Nakaoka et al., 2013;
63 Landschuetzer et al., 2014; Chen et al., 2019; Denvil-Sommer et al., 2019; Zhong et al.,
64 2020; Wang et al., 2021). However, the selection of predictors in the surface ocean
65 *p*CO₂ mapping was more empirical, focusing on the theoretical drivers of the *p*CO₂ and
66 its variation. Sea surface temperature and salinity were considered as the most
67 important and used in almost all related studies (Landschuetzer et al., 2013; Nakaoka et
68 al., 2013; Moussa et al., 2016; Laruelle et al., 2017; Zeng et al., 2017; Denvil-Sommer
69 et al., 2019), similarly the chlorophyll-a concentration is also widely used (Nakaoka et



70 al., 2013; Landschuetzer et al., 2014; Laruelle et al., 2017; Zeng et al., 2017; Denvil-
71 Sommer et al., 2019). One more indicator, mixed layer depth, appeared frequently in
72 related studies (Telszewski et al., 2009; Nakaoka et al., 2013; Landschuetzer et al., 2014;
73 Zeng et al., 2017; Denvil-Sommer et al., 2019). Besides, the sampling information have
74 been also used as indicators, including latitude and longitude (Friedrich and Oschlies,
75 2009; Jo et al., 2012; Zeng et al., 2015; Zeng et al., 2017; Denvil-Sommer et al., 2019),
76 and sampling time (Friedrich and Oschlies, 2009; Zeng et al., 2015). In recent
77 researches, dry air mixing ratio of atmospheric CO₂ (xCO₂) was also used as a
78 predicator (Landschuetzer et al., 2014; Denvil-Sommer et al., 2019). The sea surface
79 height, which was considered effective in improving the spatial pattern and the accuracy
80 of surface ocean *p*CO₂ mapping at the basin and regional scale, and the monthly
81 anomalies of the most widely used parameters mentioned above were used by the
82 Denvil-Sommer et al (2019). In the research focused on the surface ocean *p*CO₂
83 mapping of coastal areas, the bathymetry, sea ice and wind speed were also used as
84 indicators (Laruelle et al., 2017). In each of these researches, same combination of
85 indicators was applied in all areas of the global ocean, although the global ocean was
86 divided into several biogeochemical provinces in some of the researches. However, the
87 indicator that plays an important role in the surface ocean *p*CO₂ reconstruction at one
88 region may be not a good predicator of surface ocean *p*CO₂ in other regions, due to
89 complex and variable drivers in different regions. But no widely recognized method for
90 judging the importance of each predicator in the surface ocean *p*CO₂ mapping are
91 available yet. Thus, we attempted to construct a stepwise FFNN algorithm to rank the
92 importance of predicators and figure out the optimal combination in each
93 biogeochemical province defined by SOM, for decreasing the predication errors in the
94 surface ocean *p*CO₂ mapping.

95 **2 Methodology**

96 **2.1 Data**

97 The surface ocean fugacity of CO₂ (*f*CO₂) observation data from the Surface Ocean
98 CO₂ Atlas *f*CO₂ dataset version 2020 (SOCATv2020) (Bakker et al., 2016) was used to
99 construct the non-linear relationship between surface ocean *p*CO₂ and predicators. The
100 transition between *f*CO₂ and *p*CO₂ was following the formula (Körtzinger, 1999):

$$101 \quad f\text{CO}_2 = p\text{CO}_2 \cdot \exp\left(P \cdot \frac{B+2\delta}{RT}\right) \quad (1)$$

102 where *P* is the total atmospheric surface pressure using the National Centers for
103 Environmental Prediction (NCEP) monthly mean sea level pressure product (Dee et al.,



104 2011), and T is the absolute temperature. R is the gas constant ($8.314 \text{ J K}^{-1} \text{ mol}^{-1}$).
105 Parameters B and δ are both viral coefficients (Weiss, 1974).

106 In this work, parts of indicators was choose from previous researches of surface
107 ocean $p\text{CO}_2$ reconstruction based on machine learning methods, including sea surface
108 temperature (SST) and sea surface salinity (SSS) using the $1^\circ \times 1^\circ$ gridded product from
109 Chen et al (2017) at <http://159.226.119.60/cheng/> and the anomalies (SST_{anom} and
110 SSS_{anom}), chlorophyll-a concentration (CHL-a) and the anomaly (CHL-a_{anom}) using
111 satellite derived monthly product in 9 km resolution (Hu et al., 2012), mixed layer depth
112 (MLD) and sea surface height (SSH) and the anomalies (MLD_{anom} and SSH_{anom}) using
113 the ECCO2 cube92 daily product (Menemenlis et al., 2008), W velocity of ocean
114 currents (W_{vel}) at 5, 65, 105 and 195 m depth using the ECCO2 cube92 3-day product
115 (Menemenlis et al., 2008), dry air mixing ratio of atmospheric CO_2 ($x\text{CO}_2$) and the
116 anomaly ($x\text{CO}_2_{\text{anom}}$) from the GLOBAL VIEW marine boundary layer product
117 (GLOBALVIEW-CO2, 2011), sea ice area fraction using the monthly product from
118 ECMWF ERA Interim(Dee et al., 2011), 10 meters wind speed using the monthly
119 product from ECMWF ERA Interim (Dee et al., 2011), bathymetry from ETOPO2
120 (Commerce et al., 2006) , year and month (represented by 1-12), the total number of
121 months since January 1992 (N_{mon}), the sine of latitude and the sine and cosine of
122 longitude (sLat, sLon and cLon). In addition, 8 parameters which were only used in
123 similar previous research focused on other parameters, or were possibly related to the
124 driver of surface ocean $p\text{CO}_2$ and its variability, were selected to be tested. These
125 parameters included nitrate, phosphate, silicate and dissolved oxygen (DO) using the
126 monthly climatology product from WOA18 (Garcia et al., 2019a, b), sea level pressure
127 (SLP) and surface pressure from the ECMWF ERA Interim (Dee et al., 2011), the
128 Oceanic Nino Index (ONI) (Huang et al., 2017), the Southern Hemisphere Annular
129 Mode Index (SAM) (Marshall, G. J., 2003).

130 **2.2 Biogeochemical provinces defined by the Self-Organizing Map**

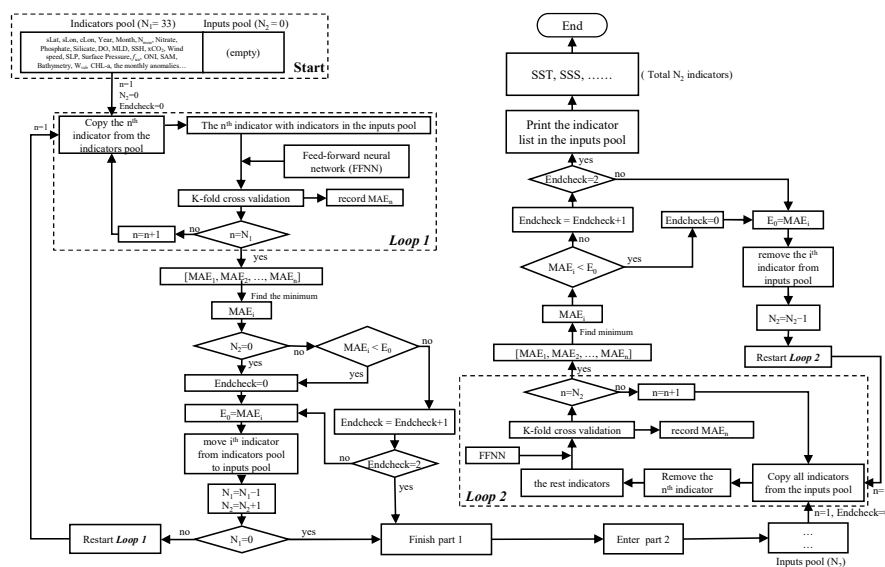
131 For applying different combination of indicators in regions based on the differences
132 in the dominated drivers of $p\text{CO}_2$ and its variability, the global ocean was divided into
133 a set of biogeochemical provinces using a Self-Organizing Map (SOM) method. The
134 monthly climatology of temperature, salinity, nitrate, phosphate, silicate, and dissolved
135 oxygen were put into a 3-by-4 size SOM networks to generate 12 biogeochemical
136 provinces, where the monthly climatology data in all 12 months were put into one SOM
137 network to generate one discrete set of biogeochemical provinces. Then the discrete
138 small “island” provinces and provinces lack of SOCAT $p\text{CO}_2$ data were merged into the



139 nearest dominated province, and the provinces covering areas separated by land were
140 further divided artificially. The final version includes total 11 biogeochemical provinces.
141 In this study the coastal area was not involved and the boundary was defined as 200m
142 depth. In addition, the $p\text{CO}_2$ mapping based on SOM defined provinces tend to be less
143 smooth near the border of different biogeochemical provinces, with obvious border line
144 appearing. However, applying of different predictors may make this problem worse. To
145 obtain a smoother distribution, we defined that the grid within $5\ 1^\circ \times 1^\circ$ grids of province
146 borders belong to all provinces adjacent to the nearest province border. Samples in these
147 grids were involved in the FFNN training process of multiple provinces, but only
148 counted once in the validation.

149 **2.3 Stepwise FFNN algorithm**

150 For finding better combination of $p\text{CO}_2$ predictors, a stepwise FFNN algorithm
151 was constructed. We used the idea of the multiple linear stepwise regression, replacing
152 the linear regression part by a Feed-forward neural networks (FFNN). The mean
153 absolute error (MAE) difference that before and after adding or removing one indicator
154 in the input of FFNN was used to estimate the performance of each indicator in the
155 FFNN predicating. Although the root mean square error (RMSE) was widely used for
156 the validation of machine learning methods. Compared to the MAE, the RMSE was
157 more sensitive to a few extreme samples, which were generally deviated far from the
158 FFNN predicting values, resulting in a huge discrepancy between the FFNN outputs
159 and $p\text{CO}_2$ observations sometimes up to hundreds of μatm . A higher weight may be put
160 on these few extreme samples than other samples in the predictor selection if the
161 performance of each indicator was estimated by RMSE in the stepwise FFNN algorithm.
162 To avoid the higher weight on these few extreme samples, the MAE was used instead
163 in the stepwise FFNN algorithm. The basic principle of the stepwise FFNN algorithm
164 was adding each indicator from a set of indicators into the inputs of FFNN and
165 removing each redundant indicator from the inputs successively to reduce the MAE
166 between the FFNN outputs and SOCAT $p\text{CO}_2$ values in the fastest way, until no
167 decrease in the MAE appearing (Fig. 1), where the indicator having no contribution to
168 reduce the prediction error was considered as redundant.



169

170

Figure 1. the procedure of stepwise FFNN algorithm

171

172

173

174

175

176

177

178

179

180

181

182

183

184

185

186

187

188

189

190

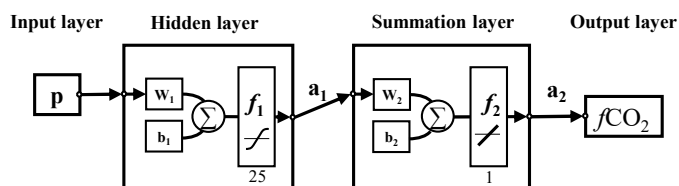
191

In the beginning of the stepwise FFNN algorithm, all available indicators were put into a matrix, referred to as indicators pool, where each of rows represents one indicator and each of columns represents one SOCAT sample. In this work we collected 33 parameters for test, that is, the indicators pool matrix has 33 rows. Meanwhile a matrix, referred to as inputs pool, was set up to storage indicators with good performance, where good performance means that adding these indicators as predictors can significantly decrease the MAE between SOCAT pCO_2 measurements and FFNN pCO_2 predictions. Then a loop of K-fold validation test run out to calculated the MAE that predicting pCO_2 by each one indicator in the indicators pool in the first step (loop 1 in the Fig. 1). Thus total 33 MAE values were obtained and the minimum was recorded as E_0 . The indicator that corresponds to the minimum of all MAE values was moved from the indicators pool to the inputs pool. After that the loop 1 restarted, i.e., the second step started with one indicator removed to the inputs pool and the rest 32 indicators waiting to be tested. Then 32 MAE values of predicting pCO_2 by each one of the rest indicators in the indicators pool with the addition of all indicators in the inputs pool were calculated out. If the MAE in the lowest situation, represented by the MAE_i , decreased compared to the E_0 , the i^{th} indicator was considered as a good indicator and was moved from the indicators pool to the inputs pool as well. Then the value of E_0 was replaced by the MAE_i . This part was repeated that the good indicators were selected out in one-by-one step and moved to the inputs pool in the way that the E_0 decreases in the fastest way, until no indicator was left in the indicators pool or no decrease can be found no



192 matter which indicator was added in the next two steps. At this time the part 1 of
193 stepwise FFNN algorithm finished, and all indicators left in the indicators pool were
194 considered redundant. The loop K-fold validation in the second part run out in a
195 opposite way that the MAE was calculated with the indicators were removed from the
196 inputs pool one by one in the way that the E_0 decreases the fastest (loop 2 in Fig. 1).
197 The second part was aimed to remove the indicator that can be represented by other
198 indicators in the inputs pool, and finished in the similar condition that no significant
199 decrease can be found no matter which indicator was removed in the next two steps.

200 The FFNN is composed of four main parts, which are namely input, hidden,
201 summation and output layer (Fig.2). The input layer is designed to pass the inputs to
202 the hidden layer and the number of neurons is equal to the dimensions of the input
203 matrix p . The hidden layer includes 25 neurons in the FFNN model, with the tan-
204 sigmoid function as the transfer function. The input p is multiplied by a matrix of
205 weights (w_1 in Fig. 2) and the inner product between the result and a bias matrix (b_1
206 Fig. 2) is calculated as the input of the transfer function in the first hidden layer. In the
207 summation layer, the transfer function f_2 is a pure linear function. The output of the
208 hidden layer is multiplied by another matrix of weights and summed. All bias and
209 weights matrixes were randomly assigned in the beginning of FFNN training. Here we
210 set one constant random number stream in the MATLAB, thus the way that the bias and
211 weights matrixes randomly assigned were steady, avoiding the appearance of
212 inconsistent results when algorithm repeats.



213
214 Figure 2. The structure of feed-forward neural network. p : input matrix; w : weighted matrix; b : bias
215 matrix; Σ : sum; f_1 : tan-sigmoid transfer function; f_2 : pure linear function; a : output matrix.

216 2.4 $p\text{CO}_2$ product

217 Dataset of parameters except CHL-a start since 1992 or earlier, while CHL-a data
218 ranges from 2002 to present. In each one of the provinces, the stepwise FFNN algorithm
219 was run out once first based on all samples covered by CHL-a data, then the algorithm
220 was run out secondly based on samples and all indicators except CHL-a and CHL-a_{anom}
221 in the year that CHL-a gridded data was not available. The $p\text{CO}_2$ mapping in the year
222 that CHL-a gridded data was not available was carried out based on the predictors
223 selected in the second run. Although the performance may improve with the number of



224 neurons increasing, the influence of number of neurons on the performance of FFNN
225 $p\text{CO}_2$ prediction remains unclear. To further decrease the predicating error between
226 FFNN outputs and SOCAT measurements, the number of neurons was improved by an
227 error test in each province. The number of neurons increased from 10 to 70 and the
228 corresponding MAE values of each size were record, and then the number of neurons
229 with lowest MAE was applied. This test avoided the appearance of insufficient learning
230 capacity for complex nonlinear relationship due to too few neurons and overfitting
231 problem due to too many neurons. Finally, based on the indicators selected by the
232 stepwise FFNN algorithm and improved FFNN size, a monthly global $1^\circ \times 1^\circ$ surface
233 ocean $p\text{CO}_2$ product from 1992 to 2019 was constructed.

234 2.5 Validation

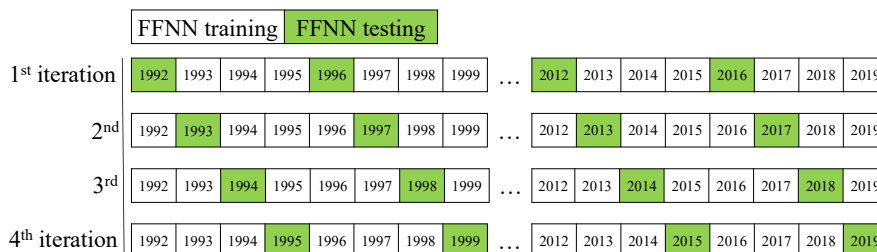
235 To better estimate the predicating error of FFNN, the MAE and additionally the
236 RMSE which was widely used in previous researches, were calculated using a K-fold
237 cross validation method. To avoid overfitting caused by a lack of independence between
238 the training samples and testing samples, the SOCAT samples were put in chronological
239 order and then divided into group of years (Table 1). In this paper, the value of K was
240 set as 4. Thus, among every 4 neighboring years, three group samples were used for
241 training FFNN model and the rest one was used for testing. Total 4 iterations were
242 carried out, where testing year changed in each iteration. After 4 iterations finished, all
243 samples have been used for testing only once, and the MAE and RMSE between FFNN
244 output and the testing samples was calculated. The performance of the predictor
245 selection algorithm was estimated by comparing the MAE and RMSE result of the
246 FFNN based on stepwise selected indicators with the result based on indicators used in
247 previous researches in each biogeochemical province (Table 2). All validation groups
248 were applied with same FFNN and same samples from SOCAT, with the only
249 differences in predictors. Same K-fold validation procedure was applied for three
250 validation groups based on different $p\text{CO}_2$ predictors. Thus, three results were
251 generated to estimate whether the stepwise FFNN algorithm can effectively find better
252 combination of $p\text{CO}_2$ predictors. Finally the $p\text{CO}_2$ data generated in all validation
253 groups were further compared with the independent observations from the Hawaii
254 Ocean Time-series (HOT) (Dore et al., 2009), Bermuda Atlantic Time-series Study
255 (BATS) (Bates, 2007) and The European Station for Time Series in the Ocean Canary
256 Islands (ESTOC) (González-Dávila and Santana-Casiano, 2009) time series station.

257
258



259

Table 1. The procedure of K-fold validation.



260

261

Table 2. validation group

Validation group	Predictor
FFNN1	Indicators selected by stepwise FFNN algorithm
FFNN2	SST, SSS, $\log_{10}(\text{MLD})$, CHL-a, xCO_2 , SST_{anom} , SSS_{anom} , $\text{xCO}_2_{\text{anom}}$, CHL-a _{anom} , $\log_{10}(\text{MLD})_{\text{anom}}$ (Landschuetzer et al., 2014)
FFNN3	SST, SSS, SSH, MLD, xCO_2 , CHL-a, SSS_{anom} , SST_{anom} , SSH_{anom} , CHL-a _{anom} , MLD_{anom} , $\text{xCO}_2_{\text{anom}}$, sLat, sLon, cLon (Denvil-Sommer et al., 2019)

262

3 Results and discussion

263

3.1 Biogeochemical provinces and corresponding predictors of $p\text{CO}_2$

264

265

266

267

268

269

270

271

272

273

274

275

276

277

278

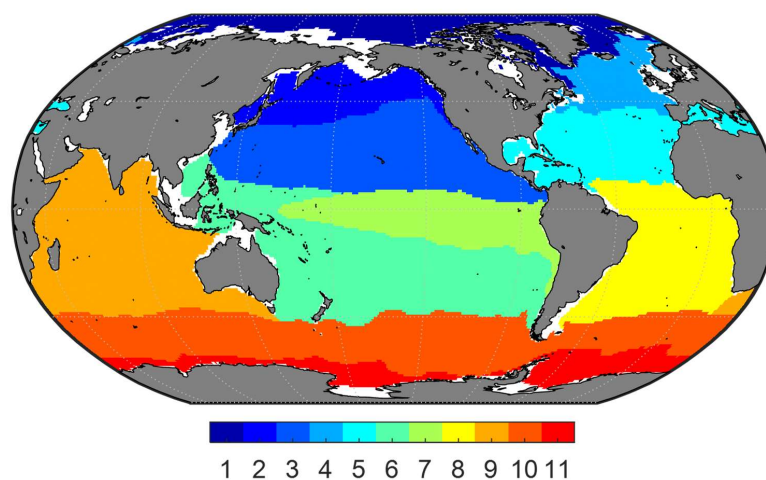
279

280

11 biogeochemical provinces generated from the SOM method after the separated small ‘island’ was removed and the province separated by lands was divided manually (Fig. 3). The results of the stepwise FFNN algorithm in each province were shown in the Table 3. The indicators were listed in the order that the stepwise FFNN algorithm printed recommended predictors out. The indicator printed earlier was relatively more recommended and played an important role in the prediction of $p\text{CO}_2$ based on FFNN. Applying of these indicators as the predictors of surface ocean $p\text{CO}_2$ effectively decreased the predicating error between the FFNN outputs and $p\text{CO}_2$ values from validation samples, thus it is reasonable to consider that these indicators were highly related to the drivers of $p\text{CO}_2$ and its variability. Indicators representing sampling position were also listed as recommended predictors in some provinces, including latitude, longitude and sampling time, suggesting that relatively steady spatial or temporal variability pattern of surface ocean $p\text{CO}_2$ existed in these biogeochemical provinces. For example, month was considered as a recommended predictor in most provinces. Especially in the provinces covering the north Atlantic Ocean (P4 and P5), the parameter month was relatively more recommended. While $p\text{CO}_2$ in these areas regularly peaked and bottomed out in summer and winter (Takahashi et al., 2009;



281 Landschutzer et al., 2016; Landschützer et al., 2020). Similarly, latitude and the sine
282 and cosine of longitude were listed as recommended predictors of $p\text{CO}_2$ in most
283 provinces, suggesting an obvious spatial distribution pattern of $p\text{CO}_2$, which was not
284 learned sufficiently by the FFNN model from existing indicators and the indicators
285 related to spatial position were applied as supplementary.



286
287

Figure 3. The map of biogeochemical provinces

288 As basic parameters highly related to the ocean environment, the temperature and
289 salinity was considered as parts of the most important predictors of surface ocean $p\text{CO}_2$,
290 and was applied in the $p\text{CO}_2$ prediction in almost all previous relating researches based
291 on various method (Jo et al., 2012; Signorini et al., 2013; Landschuetzer et al., 2014;
292 Marrec et al., 2015; Chen et al., 2016; Moussa et al., 2016; Chen et al., 2017; Laruelle
293 et al., 2017; Zeng et al., 2017; Chen et al., 2019; Denvil-Sommer et al., 2019). The
294 results of stepwise FFNN algorithm also supported this. Temperature was listed as a
295 recommended predictor in all biogeochemical provinces, suggesting that temperature
296 was the one of the most important drivers of $p\text{CO}_2$ and its variability in these provinces.
297 Similarly, the result of stepwise FFNN algorithm proved the importance of salinity in
298 the predication of $p\text{CO}_2$, which was also listed as a predictor in most provinces. In the
299 province P1 located in the Arctic, the silicate concentration and temperature were
300 considered as the most crucial predictor of $p\text{CO}_2$. The dry air mixing ratio of
301 atmospheric CO_2 ($x\text{CO}_2$) and the monthly anomaly of $x\text{CO}_2$ were also recommended
302 predictors in most of the biogeochemical provinces, suggesting that the exchange of
303 CO_2 across the sea-air interface was also an important driver of surface ocean $p\text{CO}_2$. As
304 a widely used predictor in the $p\text{CO}_2$ prediction, the chlorophyll-a concentration (CHL-



305 a) played an important role in fitting the influence of biological activities on $p\text{CO}_2$ in
 306 previous researches (Landschuetzer et al., 2014; Zeng et al., 2017; Laruelle et al., 2017;
 307 Denvil-Sommer et al., 2019). Especially in the Southern Ocean (province P10 and P11)
 308 the CHL-a was listed as the most recommended predictor in the result of stepwise
 309 FFNN algorithm. While in some other provinces (P1 and P5), the CHL-a were
 310 considered redundant that no effective decrease of MAE between FFNN outputs and
 311 $p\text{CO}_2$ measurements appeared when CHL-a data was used. Similar with the period that
 312 CHL-a was not available (represented by the subscript 'b'), the phosphate, nitrate,
 313 silicate or dissolved oxygen were recommended instead.

Table 3. Predictors in each biogeochemical province

Province	Predictors
P1	Silicate, SST, Wind speed, SSS, $\log_{10}(\text{MLD})$, SSS_{anom} , sLat, month, $W_{\text{vel}}(65\text{m})$, $\log_{10}(\text{MLD})_{\text{anom}}$, xCO_2 , cLon, Bathymetry, SSH
P2 _a *	Nitrate, CHL-a, SSS, xCO_2 , cLon, SST, $\log_{10}(\text{MLD})$, sLon, sLat, month
P2 _b *	Nitrate, $\text{xCO}_{2\text{anom}}$, sLon, SST, sLat, $\log_{10}(\text{MLD})$, cLon, SSS, SSH_{anom} , DO, $W_{\text{vel}}(195\text{m})$, Bathymetry, Silicate
P3 _a	$\log_{10}(\text{MLD})$, N_{mon} , SSH, SST, sLon, sLat, SSS, Bathymetry, month, $\log_{10}(\text{MLD})_{\text{anom}}$, cLon, Surface pressure, $W_{\text{vel}}(105\text{m})$, CHL-a, DO, SSH_{anom} , $\text{xCO}_2_{\text{anom}}$
P3 _b	$\log_{10}(\text{MLD})$, xCO_2 , sLat, sLon, SST, Surface pressure, cLon, SSS, $W_{\text{vel}}(5\text{m})$, N_{mon} , $\log_{10}(\text{MLD})_{\text{anom}}$, month, Phosphate, $\text{xCO}_2_{\text{anom}}$, $W_{\text{vel}}(105\text{m})$
P4 _a	month, sLat, cLon, SST, Year, CHL-a, DO, SSS_{anom} , $W_{\text{vel}}(195\text{m})$, SSH, $\log_{10}(\text{MLD})$, Bathymetry, SSS
P4 _b *	month, xCO_2 , DO, Wind speed, $\log_{10}(\text{MLD})$, $W_{\text{vel}}(195\text{m})$, sLon, Bathymetry, $W_{\text{vel}}(5\text{m})$, SST, Phosphate, Year, N_{mon}
P5	month, Year, SST, sLon, sLat, SSS, SST_{anom} , SSH, Bathymetry, $W_{\text{vel}}(5\text{m})$, cLon, $W_{\text{vel}}(65\text{m})$, $\log_{10}(\text{MLD})_{\text{anom}}$
P6 _a	SST, sLon, $\text{xCO}_2_{\text{anom}}$, sLat, SSS, month, Phosphate, CHL-a, $\text{CHL-a}_{\text{anom}}$, $W_{\text{vel}}(65\text{m})$, $\log_{10}(\text{MLD})_{\text{anom}}$, Nitrate, Bathymetry
P6 _b	xCO_2 , sLat, SSS, SST, Phosphate, SLP, $\text{xCO}_2_{\text{anom}}$, sLon, cLon, $W_{\text{vel}}(105\text{m})$, $W_{\text{vel}}(65\text{m})$, DO, Bathymetry, SSH, SAM
P7 _a	Nitrate, xCO_2 , sLat, SSS, SST, cLon, $\text{xCO}_2_{\text{anom}}$, $\log_{10}(\text{MLD})$, sLon, CHL-a, Phosphate, $W_{\text{vel}}(5\text{m})$, $W_{\text{vel}}(105\text{m})$, $W_{\text{vel}}(195\text{m})$
P7 _b	SST, SSS, Year, sLat, month, cLon, SSH, Bathymetry, $W_{\text{vel}}(65\text{m})$, xCO_2
P8 _a	sLat, $\text{xCO}_2_{\text{anom}}$, SSS, $\log_{10}(\text{MLD})$, CHL-a, SSH_{anom} , $W_{\text{vel}}(195\text{m})$, cLon, SST, $W_{\text{vel}}(65\text{m})$, Bathymetry, Nitrate



Province	Predictors
P8 _b	SST, xCO ₂ , cLon, sLat, SSS, Silicate, SSH, log ₁₀ (MLD), sLon
P9 _a	SST, cLon, sLat, Nitrate, W _{vel} (65m), log ₁₀ (MLD), SLP, CHL-a, Year, log ₁₀ (MLD) _{anom} , SSH _{anom}
P9 _b	SLP, month, sLon, xCO ₂ _{anom} , SST, Silicate, W _{vel} (65m)
P10 _a	CHL-a, log ₁₀ (MLD), N _{mon} , SSS, SST, Bathymetry, SSH _{anom} , W _{vel} (5m), CHL-a _{anom} , xCO ₂
P10 _b	Wind speed, xCO ₂ _{anom} , SSS, Phosphate, log ₁₀ (MLD), W _{vel} (65m), Bathymetry, SST, month
P11 _a	CHL-a, sLon, Bathymetry, SSS, SSH, SST, Nitrate, cLon, sLat
P11 _b	month, DO, SST, SSH, sLat, Nitrate, sLon, SSS, W _{vel} (195m), Silicate, SSH _{anom}

*: Due to insufficient coverage of CHL-a data in the polar areas and during the period before 2002. The $p\text{CO}_2$ data in the province that CHL-a or CHL-a_{anom} was selected as predictors was divided into two periods. The period that CHL-a data available was represented by the subscript 'a', such as P2_a, including global grids from 2002 to 2019 except polar grids in winter. The period that CHL-a data not available was represented by the subscript 'b', such as P2_b, including global grids from 1992 to 2001 and additionally some polar grids in winter from 1992 to 2019.

315 3.2 $p\text{CO}_2$ product

316 Based on the predictors given by the stepwise FFNN algorithm in each
317 biogeochemical province, a FFNN size (representing the number of neurons in the
318 hidden layer) improving validation was applied to further decrease the predication error.
319 The MAE values based on same samples and FFNN model with different number of
320 neurons were calculated, then the number of neurons corresponding to the lowest MAE
321 were applied (Fig. 4a). The MAE in most provinces tend to decrease first and then
322 increase when the number of neurons in the hidden layer of FFNN model increased
323 from 10 to 70. Based on the variation of MAE with the number of neurons in the FFNN
324 hidden layer, the optimal FFNN size in each province was considered as the number of
325 neurons when the MAE was lowest. The result and corresponding MAE were shown in
326 Fig. 4b. The MAE and RMSE of global estimates between predicted $p\text{CO}_2$ and
327 measurements from SOCAT v2020 further decreased to 11.32 and 17.99 μatm
328 respectively after applying optimal FFNN size in each province.

329

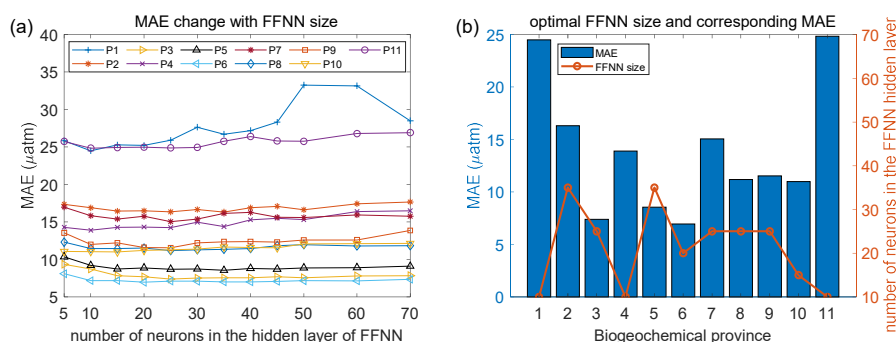
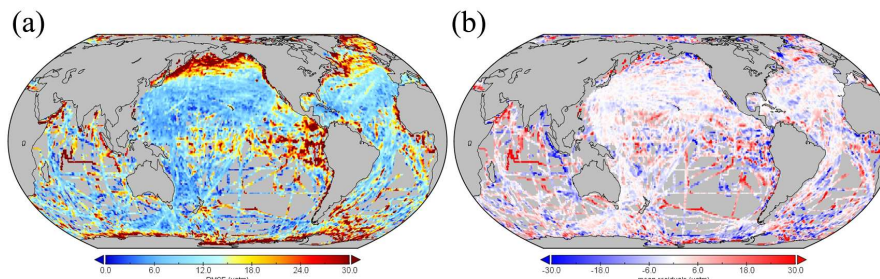


Figure 4. MAE of different FFNN size in each biogeochemical province.

330
 331
 332
 333
 334
 335
 336
 337
 338
 339

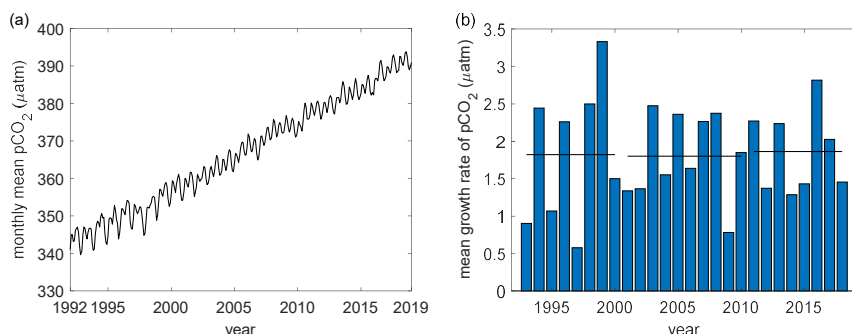
Then the RMSE and mean residuals in each grid were calculated based the K-fold cross validation method. In most grids, the RMSE was lower than 10 μatm and the mean residuals was close to zero (Fig. 5). However, the prediction error in the north subpolar Pacific, the east equatorial Pacific and the Southern Ocean near the Antarctic continent was obviously higher than other areas. Distribution of mean residuals suggested that surface ocean $p\text{CO}_2$ in the Indian Ocean tend to be overestimated by the FFNN models. While in other regions the distribution of mean residuals was more discrete and no obvious pattern was found.



340
 341
 342
 343
 344
 345
 346
 347

Figure 5. Global maps of (a) RMSE and (b) mean residuals between predicted $p\text{CO}_2$ and SOCAT observations

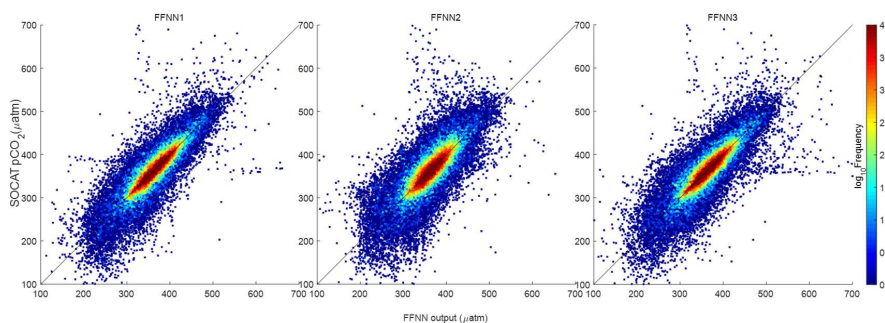
Based on stepwise FFNN algorithm and improved FFNN size in each province, a monthly $1^\circ \times 1^\circ$ grided surface ocean $p\text{CO}_2$ product from January 1992 to August 2019 was constructed. The interannual variability of global average $p\text{CO}_2$ was showed in the Fig. 6. The global open ocean average $p\text{CO}_2$ increased about 1.85 μatm per year from 1992 to 2019.



348
349 Figure 6. Interannual variability of global open-oceanic $p\text{CO}_2$ during 1992-2019. (a): global
350 monthly mean $p\text{CO}_2$, (b): growth rate of global monthly mean $p\text{CO}_2$

351 3.3 Validation of the stepwise FFNN algorithm based on SOCAT samples

352 Validation based on the K-fold cross validation method suggested that most FFNN
353 outputs were quite close to the $p\text{CO}_2$ values from SOCAT v2020 samples (Fig. 7).
354 Comparing the results based on different combination of predictors, the results of
355 FFNN1 (based on stepwise FFNN algorithm, this paper) and FFNN3 (based on 15
356 predictors from Denvil-Sommer, et al. 2019) were obviously more precise than that of
357 FFNN2 (based on 10 predictors from Landschuetzer, et al. 2014). Where the plots in
358 the result of FFNN1 was most concentrated along the $y=x$ line, suggesting extremely
359 close FFNN outputs with the measured $p\text{CO}_2$ values from SOCAT, with the RMSE of
360 17.99 μatm in the global open oceans. The RMSE of FFNN1 was lower than that of
361 FFNN2 (22.95 μatm) and FFNN3 (19.17 μatm).



362
363 Figure 7. Comparing of FFNN predicted $p\text{CO}_2$ with SOCAT $p\text{CO}_2$. FFNN1 was based on predictors
364 selected by the stepwise-FFNN algorithm. FFNN2 and FFNN3 were based on predictors from
365 Landschuetzer et al., 2014 and Denvil-Sommer et al., 2019 respectively.

366 For specific comparison of accuracy in each province, the MAE of FFNN1 was
367 lower in most provinces (Table. 4), except the relatively close results between the
368 FFNN1 and FFNN3 in parts of provinces. Where the MAE of FFNN1 in the province



369 P9 was significantly lower than that of the other validation groups, suggesting a better
 370 combination of predictors highly related to the drivers of surface ocean $p\text{CO}_2$ and its
 371 variability in the Indian Ocean. Compared with predictors of FFNN2 and FFNN3, the
 372 predictors of FFNN1 added surface pressure and W velocity of ocean currents, and
 373 abandoned the monthly anomalies of other indicators in the province P9. The low
 374 relevance between part of the monthly anomalies, such as SSS_{anom} and SSH_{anom} , may
 375 be responsible for significant lower MAE of FFNN1. Adding redundant indicators may
 376 cause misleading in the learning of FFNN model on the contrary. The MAE and RMSE
 377 difference between FFNN1 and FFNN3 in some provinces were relatively small,
 378 because predictors used in both FFNN1 and FFNN3 were related to main drivers of
 379 $p\text{CO}_2$, such as CHL-a, $x\text{CO}_2$ and MLD.

380 Table 4. Performance of the $p\text{CO}_2$ prediction based on different predictors

Province	FFNN size	MAE (μatm)			RMSE (μatm)		
		FFNN1	FFNN2	FFNN3	FFNN1	FFNN2	FFNN3
P1 (9856)	10	24.50	32.32	26.87	32.27	43.68	35.08
P2 (30516)	35	16.32	20.63	16.67	24.32	29.87	25.03
P3 (56367)	25	7.39	12.16	7.95	11.33	17.75	11.88
P4 (29595)	10	13.89	16.91	14.73	21.06	24.29	22.27
P5 (45358)	35	8.55	12.28	9.00	12.80	17.86	13.72
P6 (31803)	20	6.96	9.94	7.24	9.86	14.64	11.00
P7 (11233)	25	15.05	19.55	15.49	20.98	27.61	21.10
P8 (10259)	25	11.19	15.07	12.43	17.10	20.87	17.66
P9 (7440)	25	11.54	13.78	15.49	17.15	22.89	28.29
P10 (21206)	15	11.00	11.76	12.14	16.61	17.22	17.66
P11 (10683)	10	24.84	29.26	25.74	34.73	40.42	35.22
Global (264316)		11.32	15.08	12.06	17.99	22.95	19.17

381 (FFNN1 was based on predictors selected by the stepwise-FFNN algorithm. FFNN2 and FFNN3
 382 were based on predictors from Landschuetzer et al., 2014 and Denvil-Sommer et al., 2019
 383 respectively.)

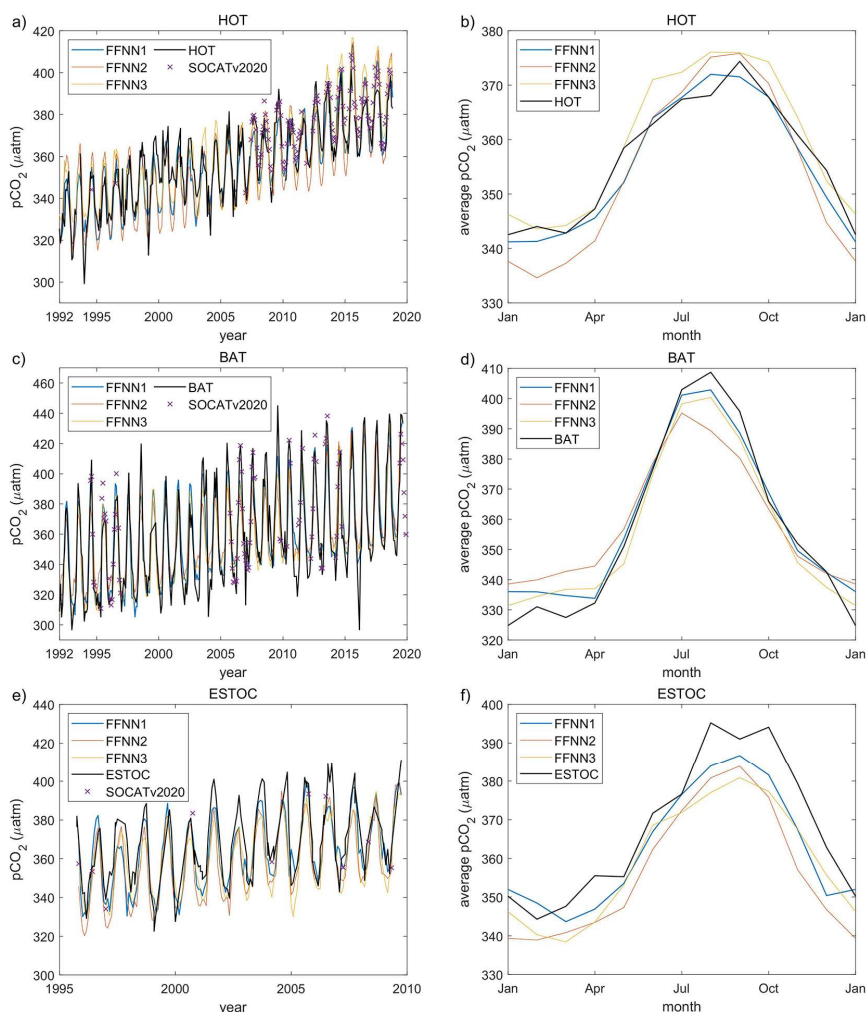
384

385 3.4 Validation based on independent observations

386 The FFNN outputs based on different combination of predictors were compared
 387 with independent observations from the Ocean Time-series (HOT) (Dore et al., 2009),



388 Bermuda Atlantic Time-series Study (BATS) (Bates, 2007) and The European Station
389 for Time Series in the Ocean Canary Islands (ESTOC) (González-Dávila and Santana-
390 Casiano, 2009) (Fig. 8). The interannual variability and seasonal pattern of $p\text{CO}_2$ in the
391 grids the HOT station located from different validation groups were similar and close
392 to the observations from the HOT, which was located in the province P3. From 1992 to
393 2019, the RMSE between FFNN1 outputs and HOT observations was only $9.29 \mu\text{atm}$,
394 lower than the $10.85 \mu\text{atm}$ of FFNN2 and the $10.70 \mu\text{atm}$ of FFNN3. The monthly mean
395 $p\text{CO}_2$ of FFNN2 during winter was obviously lower than the HOT observations and
396 $p\text{CO}_2$ values of other validation groups, while the FFNN1 and FFNN3 outputs were
397 closer to the HOT observations. MAE between predicted $p\text{CO}_2$ and HOT observations
398 were also lower in the validation group FFNN1, which was only $7.17 \mu\text{atm}$, compared
399 to the $8.61 \mu\text{atm}$ of FFNN2 and the $8.44 \mu\text{atm}$ of FFNN3. Higher bias generated in the
400 winter bottom and summer peak, which was showed more obviously in the monthly
401 average of $p\text{CO}_2$ (Fig. 8b). Compared with other validation groups, the result of FFNN1
402 was closer to the monthly average values of the HOT observations. Same conclusion
403 can be obtained in the ESTOC and BATS station located in the province P5. The RMSE
404 between FFNN1 outputs and independent observations were $13.03 \mu\text{atm}$ in the BATS
405 station and $11.35 \mu\text{atm}$ in the ESTOC station, lower than that of other validation groups.
406 The RMSE between FFNN2 outputs and independent observations was $16.15 \mu\text{atm}$ in
407 the BATS station and $14.51 \mu\text{atm}$ in the ESTOC station. For the group FFNN3, the
408 RMSE was $13.09 \mu\text{atm}$ in the BATS station and $13.01 \mu\text{atm}$ in the ESTOC station. All
409 results were extremely close to the independent observations, but the RMSE and MAE
410 of FFNN1 were lower. Similar with the situation in the HOT station, the FFNN1 was
411 most close and the FFNN3 second. Based on the better performance of FFNN1, in
412 which the predictors selected by stepwise FFNN algorithm were used, we may
413 conclude that the stepwise FFNN algorithm can effectively find better combination of
414 predictors to fit the diver of surface ocean $p\text{CO}_2$ and obtained lower error.



415

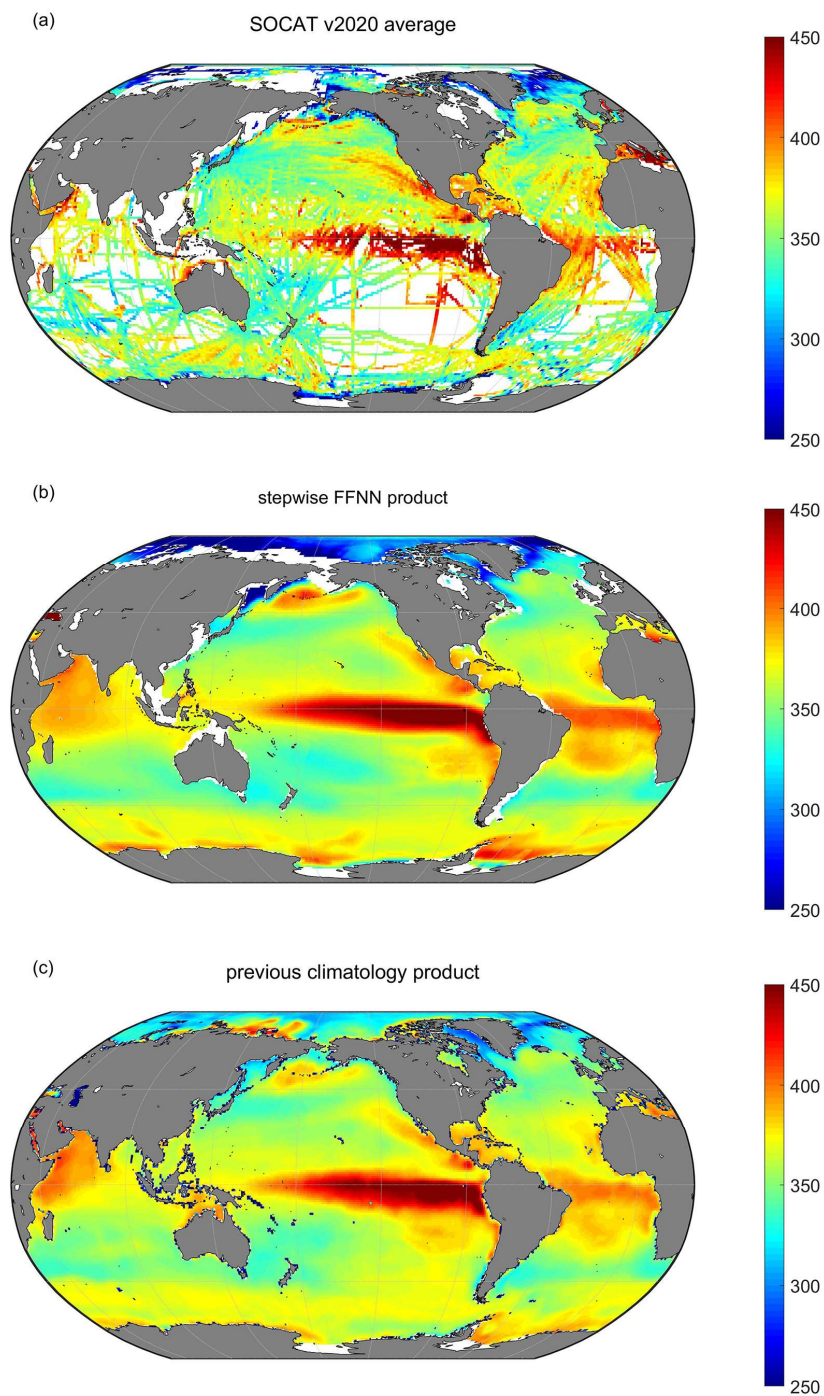
416 Figure 8. Validation based on independent observation from time series stations. a) and b): the
417 Hawaii Ocean Time-series (HOT) (Dore et al., 2009); c) and d): the Bermuda Atlantic Time-series
418 Study (BATS) (Bates, 2007); e) and f): the European Station for Time Series in the Ocean Canary
419 Islands (ESTOC) (González-Dávila and Santana-Casiano, 2009) time series station. FFNN1 was
420 based on predictors selected by the stepwise-FFNN algorithm. FFNN2 and FFNN3 were based on
421 predictors from Landschuetzer et al., 2014 and Denvil-Sommer et al., 2019 respectively.
422 SOCATv2020 represents the monthly mean $p\text{CO}_2$ of SOCAT observations in the corresponding
423 grids of each time series station.

424 3.5 Climatological spatial distribution

425 The climatological average distribution of $p\text{CO}_2$ suggested a significant spatial
426 variability (Fig. 9), which is consistent with the average distribution of SOCAT



427 observations. In the Pacific Ocean, the high $p\text{CO}_2$ areas showed by the stepwise-FFNN
428 product (Fig. 9b), including the equatorial areas, east temperate areas and north
429 subpolar areas, were highly consistent with the SOCAT datasets (Fig. 9a). Similarly, the
430 distribution of $p\text{CO}_2$ in the Atlantic Ocean and the Indian Ocean was also close.
431 However, the stepwise-FFNN product suggested lower $p\text{CO}_2$ average values in the
432 Arctic and higher values in the Southern Ocean near the Antarctic continent. Compared
433 with previous climatology product (Landschützer et al., 2020), the global distribution
434 pattern of surface ocean $p\text{CO}_2$ was basically well consistent. Inconsistent spatial
435 distribution also existed in the Arctic and parts of the Southern Ocean near the Antarctic
436 continent. The differences between stepwise-FFNN product and previous climatology
437 product may be caused by differences in methods or SOCAT dataset versions used.
438 While lower average values of the SOCAT dataset in the Southern Ocean may be caused
439 by the undersampling in winter. The global spatial distribution pattern of the stepwise
440 FFNN $p\text{CO}_2$ product was basically well consistent with previous climatology product
441 and SOCAT dataset, suggesting that $p\text{CO}_2$ predicting based on regional different
442 predictors selected by the stepwise FFNN algorithm was credible.



443
444 Figure 9. Comparison between long term average of a): SOCAT v2020 dataset, b): the stepwise
445 FFNN $p\text{CO}_2$ product and c): previous climatology product adapted from Landschützer et al., 2020.



446 **4. Conclusions**

447 A stepwise FFNN algorithm was constructed to decreasing the predicating error in
448 the surface ocean $p\text{CO}_2$ mapping by finding better combinations of $p\text{CO}_2$ predictors in
449 each biogeochemical province defined by SOM method. Comparing with the
450 performance of FFNN based on predictors same with previous researches, the RMSE
451 decreased when using predictors selected by the stepwise FFNN algorithm in all
452 provinces, suggesting that the stepwise FFNN algorithm was capable to find better
453 combination of predictors. In addition, validation based on independent observations
454 from HOT, BATS and ESTOC time series stations also proved the better performance
455 of FFNN based on predictors selected by the stepwise FFNN algorithm. We further
456 decreased the MAE and RMSE of global estimates to 11.32 and 17.99 μatm by
457 improving the number of neurons in the hidden layer of FFNN. Then a monthly $1^\circ \times 1^\circ$
458 gridded global open-oceanic surface ocean $p\text{CO}_2$ product from January 1992 to August
459 2019 was constructed, based improved FFNN size and the predictors selected by
460 stepwise FFNN algorithm. In this study, regional specific combination of predictors
461 was first applied in the global surface ocean $p\text{CO}_2$ mapping. The result of the stepwise
462 FFNN algorithm was also capable for analyzes of driving based on the ranking of
463 relative importance of each predictor. The more important predictor, which played a
464 more important role in decreasing the predicting error, will be selected earlier and listed
465 at the front of the recommended predictor list. In the future work, the stepwise FFNN
466 algorithm will be attempted in the mapping of other parameters, such as total alkalinity
467 and pH, to provide more sufficient data support for studies on ocean acidification and
468 carbon cycling.

469 **Code and data availability**

470 The stepwise FFNN algorithm (as a .m file for MATLAB) and the global $1^\circ \times 1^\circ$
471 gridded surface ocean $p\text{CO}_2$ product since from January 1992 to August 2019 (as a
472 NetCDF file) generated during this study is available from the Institute of Oceanology
473 of the Chinese Academy of Sciences Marine Science Data Center at
474 <http://dx.doi.org/10.12157/iocas.2021.0022>.

475 **Author contribution**

476 Ma Jun, Yuan Huamao and Duan Liqin collected the dataset of $p\text{CO}_2$ predictors,
477 and Qu baoxiao and Wang Yanjun was contributed in the synthesis of datasets. Zhong
478 Guorong, Li Xuegang and Song Jinming designed the predictor selection algorithm
479 and performed the reconstruction of $p\text{CO}_2$ product. Wang Fan, Zhang Bin, Sun Xiaoxia,
480 Zhang Wuchang, and Wang Zhenyan were contributed in the further improving. Zhong



481 Guorong prepared the manuscript with contributions from all co-authors.

482 **Competing interests**

483 The authors declare that they have no conflict of interest.

484 **Acknowledgement**

485 This work was supported by The National Key Research and Development
486 Program of China (No. 2017YFA0603204), the Strategic Priority Research Program of
487 the Chinese Academy of Sciences (No. XDA19060401), National Natural Science
488 Foundation of China (No. 91958103 and No. 42176200), and Natural Science
489 Foundation of Shandong Province (ZR2020YQ28). We thank SOCAT for sharing the
490 $f\text{CO}_2$ observation data. The Surface Ocean CO_2 Atlas (SOCAT) is an international effort,
491 endorsed by the International Ocean Carbon Coordination Project (IOCCP), the Surface
492 Ocean Lower Atmosphere Study (SOLAS) and the Integrated Marine Biosphere
493 Research (IMBeR) program, to deliver a uniformly quality-controlled surface ocean
494 CO_2 database. The many researchers and funding agencies responsible for the collection
495 of data and quality control are thanked for their contributions to SOCAT.

496

497 **References**

- 498 Bakker, D. C. E., Pfeil, B., Landa, C. S., Metzl, N., O'Brien, K. M., Olsen, A., Smith,
499 K., Cosca, C., Harasawa, S., Jones, S. D., Nakaoka, S.-i., Nojiri, Y., Schuster, U.,
500 Steinhoff, T., Sweeney, C., Takahashi, T., Tilbrook, B., Wada, C., Wanninkhof, R.,
501 Alin, S. R., Balestrini, C. F., Barbero, L., Bates, N. R., Bianchi, A. A., Bonou, F.,
502 Boutin, J., Bozec, Y., Burger, E. F., Cai, W.-J., Castle, R. D., Chen, L., Chierici, M.,
503 Currie, K., Evans, W., Featherstone, C., Feely, R. A., Fransson, A., Goyet, C.,
504 Greenwood, N., Gregor, L., Hankin, S., Hardman-Mountford, N. J., Harlay, J.,
505 Hauck, J., Hoppema, M., Humphreys, M. P., Hunt, C., Huss, B., Ibanhez, J. S. P.,
506 Johannessen, T., Keeling, R., Kitidis, V., Koertzing, A., Kozyr, A.,
507 Krasakopoulou, E., Kuwata, A., Landschuetzer, P., Lauvset, S. K., Lefevre, N., Lo
508 Monaco, C., Manke, A., Mathis, J. T., Merlivat, L., Millero, F. J., Monteiro, P. M.
509 S., Munro, D. R., Murata, A., Newberger, T., Omar, A. M., Ono, T., Paterson, K.,
510 Pearce, D., Pierrot, D., Robbins, L. L., Saito, S., Salisbury, J., Schlitzer, R.,
511 Schneider, B., Schweitzer, R., Sieger, R., Skjelvan, I., Sullivan, K. F., Sutherland, S.
512 C., Sutton, A. J., Tadokoro, K., Telszewski, M., Tuma, M., van Heuven, S. M. A.
513 C., Vandemark, D., Ward, B., Watson, A. J., and Xu, S.: A multi-decade record of
514 high-quality $f\text{CO}_2$ data in version 3 of the Surface Ocean CO_2 Atlas (SOCAT),
515 Earth System Science Data, 8, 383-413, 10.5194/essd-8-383-2016, 2016.
- 516 Bates, N. R.: Interannual variability of the oceanic CO_2 sink in the subtropical gyre of
517 the North Atlantic Ocean over the last 2 decades, Journal of Geophysical Research:
518 Oceans, 112, 2007.
- 519 Chen, L. Q., Xu, S. Q., Gao, Z. Y., Chen, H. Y., Zhang, Y. H., Zhan, J. Q., and Li, W.:
520 Estimation of monthly air-sea CO_2 flux in the southern Atlantic and Indian Ocean
521 using in-situ and remotely sensed data, Remote Sensing of Environment, 115,
522 1935-1941, 10.1016/j.rse.2011.03.016, 2011.



- 523 Chen, S., Hu, C., Barnes, B. B., Wanninkhof, R., Cai, W.-J., Barbero, L., and Pierrot,
524 D.: A machine learning approach to estimate surface ocean $p\text{CO}_2$ from satellite
525 measurements, *Remote Sensing of Environment*, 228, 203-226,
526 10.1016/j.rse.2019.04.019, 2019.
- 527 Chen, S. L., Hu, C. M., Byrne, R. H., Robbins, L. L., and Yang, B.: Remote
528 estimation of surface $p\text{CO}_2$ on the West Florida Shelf, *Continental Shelf Research*,
529 128, 10-25, 10.1016/j.csr.2016.09.004, 2016.
- 530 Chen, S. L., Hu, C. M., Cai, W. J., and Yang, B.: Estimating surface $p\text{CO}_2$ in the
531 northern Gulf of Mexico: Which remote sensing model to use?, *Continental Shelf*
532 *Research*, 151, 94-110, 10.1016/j.csr.2017.10.013, 2017.
- 533 Commerce, U. D. o., Administration, N. O. a. A., and Center, N. G. D.: 2-minute
534 Gridded Global Relief Data (ETOPO2v2).
535 <http://www.ngdc.noaa.gov/mgg/fliers/06mgg01.html>, 2006.
- 536 Dee, D. P., Uppala, S. M., Simmons, A. J., Berrisford, P., Poli, P., Kobayashi, S.,
537 Andrae, U., Balmaseda, M. A., Balsamo, G., Bauer, P., Bechtold, P., Beljaars, A. C.
538 M., van de Berg, L., Bidlot, J., Bormann, N., Delsol, C., Dragani, R., Fuentes, M.,
539 Geer, A. J., Haimberger, L., Healy, S. B., Hersbach, H., Holm, E. V., Isaksen, L.,
540 Kallberg, P., Kohler, M., Matricardi, M., McNally, A. P., Monge-Sanz, B. M.,
541 Morcrette, J. J., Park, B. K., Peubey, C., de Rosnay, P., Tavolato, C., Thepaut, J. N.,
542 and Vitart, F.: The ERA-Interim reanalysis: configuration and performance of the
543 data assimilation system, *Q J Roy Meteor Soc*, 137, 553-597, 10.1002/qj.828, 2011.
- 544 Denvil-Sommer, A., Gehlen, M., Vrac, M., and Mejia, C.: LSCE-FFNN-v1: a two-
545 step neural network model for the reconstruction of surface ocean $p\text{CO}_2$ over the
546 global ocean, *Geoscientific Model Development*, 12, 2091-2105, 10.5194/gmd-12-
547 2091-2019, 2019.
- 548 Dore, J. E., Lukas, R., Sadler, D. W., Church, M. J., and Karl, D. M.: Physical and
549 biogeochemical modulation of ocean acidification in the central North Pacific,
550 *Proceedings of the National Academy of Sciences*, 106, 12235-12240, 2009.
- 551 Friedlingstein, P., Jones, M. W., O'Sullivan, M., Andrew, R. M., Hauck, J., Peters, G.
552 P., Peters, W., Pongratz, J., Sitch, S., Le Quere, C., Bakker, D. C. E., Canadell, J.
553 G., Ciais, P., Jackson, R. B., Anthoni, P., Barbero, L., Bastos, A., Bastrikov, V.,
554 Becker, M., Bopp, L., Buitenhuis, E., Chandra, N., Chevallier, F., Chini, L. P.,
555 Currie, K. I., Feely, R. A., Gehlen, M., Gilfillan, D., Gkritzalis, T., Goll, D. S.,
556 Gruber, N., Gutekunst, S., Harris, I., Haverd, V., Houghton, R. A., Hurtt, G., Ilyina,
557 T., Jain, A. K., Joetzer, E., Kaplan, J. O., Kato, E., Goldewijk, K. K., Korsbakken,
558 J. I., Landschuetzer, P., Lauvset, S. K., Lefevre, N., Lenton, A., Lienert, S.,
559 Lombardozi, D., Marland, G., McGuire, P. C., Melton, J. R., Metzl, N., Munro, D.
560 R., Nabel, J. E. M. S., Nakaoka, S.-I., Neill, C., Omar, A. M., Ono, T., Pregon, A.,
561 Pierrot, D., Poulter, B., Rehder, G., Resplandy, L., Robertson, E., Rodenbeck, C.,
562 Seferian, R., Schwinger, J., Smith, N., Tans, P. P., Tian, H., Tilbrook, B., Tubiello,
563 F. N., van der Werf, G. R., Wiltshire, A. J., and Zaehle, S.: Global Carbon Budget
564 2019, *Earth System Science Data*, 11, 1783-1838, 10.5194/essd-11-1783-2019,
565 2019.



- 566 Friedrich, T., and Oschlies, A.: Neural network-based estimates of North Atlantic
567 surface $p\text{CO}_2$ from satellite data: A methodological study, *Journal of Geophysical*
568 *Research-Oceans*, 114, Artn C03020, 10.1029/2007jc004646, 2009.
- 569 Garcia, H., Weathers, K., Paver, C., Smolyar, I., Boyer, T., Locarnini, M., Zweng, M.,
570 Mishonov, A., Baranova, O., and Seidov, D.: *World Ocean Atlas 2018. Vol. 4:*
571 *Dissolved Inorganic Nutrients (phosphate, nitrate and nitrate+ nitrite, silicate),*
572 2019a.
- 573 Garcia, H., Weathers, K., Paver, C., Smolyar, I., Boyer, T., Locarnini, M., Zweng, M.,
574 Mishonov, A., Baranova, O., and Seidov, D.: *World Ocean Atlas 2018, Volume 3:*
575 *Dissolved Oxygen, Apparent Oxygen Utilization, and Dissolved Oxygen*
576 *Saturation, 2019b.*
- 577 GLOBALVIEW-CO2: Cooperative Atmospheric Data Integration Project - Carbon
578 Dioxide [CD-ROM]. NOAA ESRL, B., Colo. (Ed.), [Available at
579 <ftp.cmdl.noaa.gov>, path: [cgg/co2/GLOBALVIEW](ftp://ftp.cmdl.noaa.gov/cg/co2/GLOBALVIEW), 5th January 2013.], 2011.
- 580 González-Dávila, M., and Santana-Casiano, J.: Sea surface and atmospheric $f\text{CO}_2$ data
581 measured during the estoc time series cruises from 1995-2009, CDIAC, Oak Ridge
582 National Laboratory, US Department of Energy, Oak Ridge, Tennessee. doi, 10,
583 2009.
- 584 Hales, B., Strutton, P. G., Saraceno, M., Letelier, R., Takahashi, T., Feely, R., Sabine,
585 C., and Chavez, F.: Satellite-based prediction of $p\text{CO}_2$ in coastal waters of the
586 eastern North Pacific, *Prog Oceanogr*, 103, 1-15, 10.1016/j.pocean.2012.03.001,
587 2012.
- 588 Hu, C., Lee, Z., and Franz, B.: Chlorophyll a algorithms for oligotrophic oceans: A
589 novel approach based on three-band reflectance difference, *Journal of Geophysical*
590 *Research: Oceans*, 117, 10.1029/2011jc007395, 2012.
- 591 Huang, B., Thorne, P. W., Banzon, V. F., Boyer, T., Chepurin, G., Lawrimore, J. H.,
592 Menne, M. J., Smith, T. M., Vose, R. S., and Zhang, H.-M.: Extended reconstructed
593 sea surface temperature, version 5 (ERSSTv5): upgrades, validations, and
594 intercomparisons, *J Climate*, 30, 8179-8205, 2017.
- 595 Ishii, M., Feely, R. A., Rodgers, K. B., Park, G. H., Wanninkhof, R., Sasano, D.,
596 Sugimoto, H., Cosca, C. E., Nakaoka, S., Telszewski, M., Nojiri, Y., Fletcher, S. E.
597 M., Niwa, Y., Patra, P. K., Valsala, V., Nakano, H., Lima, I., Doney, S. C.,
598 Buitenhuis, E. T., Aumont, O., Dunne, J. P., Lenton, A., and Takahashi, T.: Air-sea
599 CO_2 flux in the Pacific Ocean for the period 1990-2009, *Biogeosciences*, 11, 709-
600 734, 10.5194/bg-11-709-2014, 2014.
- 601 Jo, Y. H., Dai, M. H., Zhai, W. D., Yan, X. H., and Shang, S. L.: On the variations of
602 sea surface $p\text{CO}_2$ in the northern South China Sea: A remote sensing based neural
603 network approach, *Journal of Geophysical Research-Oceans*, 117, Artn C08022,
604 10.1029/2011jc007745, 2012.
- 605 Keppler, L., and Landschutzer, P.: Regional Wind Variability Modulates the Southern
606 Ocean Carbon Sink, *Scientific Reports*, 9, ARTN 7384, 10.1038/s41598-019-
607 43826-y, 2019.
- 608 Körtzinger, A.: Determination of carbon dioxide partial pressure ($p\text{CO}_2$), 3rd ed.,
609 *Methods of Seawater Analysis*, 3rd edn., 1999.



- 610 Landschuetzer, P., Gruber, N., Bakker, D. C. E., and Schuster, U.: Recent variability
611 of the global ocean carbon sink, *Glob. Biogeochem. Cycle*, 28, 927-949,
612 10.1002/2014gb004853, 2014.
- 613 Landschuetzer, P., Gruber, N., Bakker, D. C. E., Schuster, U., Nakaoka, S., Payne, M.
614 R., Sasse, T. P., and Zeng, J.: A neural network-based estimate of the seasonal to
615 inter-annual variability of the Atlantic Ocean carbon sink, *Biogeosciences*, 10,
616 7793-7815, 10.5194/bg-10-7793-2013, 2013.
- 617 Landschuetzer, P., Gruber, N., Haumann, A., Rodenbeck, C., Bakker, D. C. E., van
618 Heuven, S., Hoppema, M., Metzl, N., Sweeney, C., Takahashi, T., Tilbrook, B., and
619 Wanninkhof, R.: The reinvigoration of the Southern Ocean carbon sink, *Science*,
620 349, 1221-1224, 10.1126/science.aab2620, 2015.
- 621 Landschuetzer, P., Gruber, N., and Bakker, D. C. E.: Decadal variations and trends of
622 the global ocean carbon sink, *Glob. Biogeochem. Cycle*, 30, 1396-1417,
623 10.1002/2015gb005359, 2016.
- 624 Landschuetzer, P., Laruelle, G. G., Roobaert, A., and Regnier, P.: A uniform $p\text{CO}_2$
625 climatology combining open and coastal oceans, *Earth Syst. Sci. Data Discuss.*,
626 2020, 1-30, 10.5194/essd-2020-90, 2020.
- 627 Laruelle, G. G., Landschuetzer, P., Gruber, N., Tison, J. L., Delille, B., and Regnier, P.:
628 Global high-resolution monthly $p\text{CO}_2$ climatology for the coastal ocean derived
629 from neural network interpolation, *Biogeosciences*, 14, 4545-4561, 10.5194/bg-14-
630 4545-2017, 2017.
- 631 Marrec, P., Cariou, T., Mace, E., Morin, P., Salt, L. A., Vernet, M., Taylor, B., Paxman,
632 K., and Bozec, Y.: Dynamics of air-sea CO_2 fluxes in the northwestern European
633 shelf based on voluntary observing ship and satellite observations, *Biogeosciences*,
634 12, 5371-5391, 10.5194/bg-12-5371-2015, 2015.
- 635 Marshall G J.: Trends in the Southern Annular Mode from observations and
636 reanalyses, *Journal of climate*, 16, 10.1175/1520-
637 0442(2003)016<4134:TITSAM>2.0.CO;2, 4134-4143, 2003.
- 638 Menemenlis, D., Campin, J.-M., Heimbach, P., Hill, C., Lee, T., Nguyen, A.,
639 Schodlok, M., and Zhang, H.: ECCO2: High Resolution Global Ocean and Sea Ice
640 Data Synthesis, *Mercator Ocean Quarterly Newsletter*, 2008.
- 641 Moussa, H., Benallal, M. A., Goyet, C., and Lefevre, N.: Satellite-derived CO_2
642 fugacity in surface seawater of the tropical Atlantic Ocean using a feedforward
643 neural network, *Int J Remote Sens*, 37, 580-598, 10.1080/01431161.2015.1131872,
644 2016.
- 645 Nakaoka, S., Telszewski, M., Nojiri, Y., Yasunaka, S., Miyazaki, C., Mukai, H., and
646 Usui, N.: Estimating temporal and spatial variation of ocean surface $p\text{CO}_2$ in the
647 North Pacific using a self-organizing map neural network technique,
648 *Biogeosciences*, 10, 6093-6106, 10.5194/bg-10-6093-2013, 2013.
- 649 Regnier, P., Friedlingstein, P., Ciais, P., Mackenzie, F. T., Gruber, N., Janssens, I. A.,
650 Laruelle, G. G., Lauerwald, R., Luyssaert, S., Andersson, A. J., Arndt, S., Arnosti,
651 C., Borges, A. V., Dale, A. W., Gallego-Sala, A., Godderis, Y., Goossens, N.,
652 Hartmann, J., Heinze, C., Ilyina, T., Joos, F., LaRowe, D. E., Leifeld, J., Meysman,
653 F. J. R., Munhoven, G., Raymond, P. A., Spahni, R., Suntharalingam, P., and



- 654 Thullner, M.: Anthropogenic perturbation of the carbon fluxes from land to ocean,
655 Nature Geoscience, 6, 597-607, 10.1038/Ngeo1830, 2013.
- 656 Sabine, C. L., Feely, R. A., Gruber, N., Key, R. M., Lee, K., Bullister, J. L.,
657 Wanninkhof, R., Wong, C. S., Wallace, D. W. R., Tilbrook, B., Millero, F. J., Peng,
658 T. H., Kozyr, A., Ono, T., and Rios, A. F.: The oceanic sink for anthropogenic CO₂,
659 Science, 305, 367-371, DOI 10.1126/science.1097403, 2004.
- 660 Sarma, V. V. S. S.: Monthly variability in surface *p*CO₂ and net air-sea CO₂ flux in the
661 Arabian Sea, Journal of Geophysical Research-Oceans, 108, Artn 3255,
662 10.1029/2001jc001062, 2003.
- 663 Sarma, V. V. S. S., Saino, T., Sasaoka, K., Nojiri, Y., Ono, T., Ishii, M., Inoue, H. Y.,
664 and Matsumoto, K.: Basin-scale *p*CO₂ distribution using satellite sea surface
665 temperature, Chl-a, and climatological salinity in the North Pacific in spring and
666 summer, Glob. Biogeochem. Cycle, 20, Artn Gb3005, 10.1029/2005gb002594,
667 2006.
- 668 Schuster, U., McKinley, G. A., Bates, N., Chevallier, F., Doney, S. C., Fay, A. R.,
669 Gonzalez-Davila, M., Gruber, N., Jones, S., Krijnen, J., Landschuetzer, P., Lefevre,
670 N., Manizza, M., Mathis, J., Metzl, N., Olsen, A., Rios, A. F., Roedenbeck, C.,
671 Santana-Casiano, J. M., Takahashi, T., Wanninkhof, R., and Watson, A. J.: An
672 assessment of the Atlantic and Arctic sea-air CO₂ fluxes, 1990-2009,
673 Biogeosciences, 10, 607-627, 10.5194/bg-10-607-2013, 2013.
- 674 Shadwick, E. H., Thomas, H., Comeau, A., Craig, S. E., Hunt, C. W., and Salisbury, J.
675 E.: Air-Sea CO₂ fluxes on the Scotian Shelf: seasonal to multi-annual variability,
676 Biogeosciences, 7, 3851-3867, 10.5194/bg-7-3851-2010, 2010.
- 677 Signorini, S. R., Mannino, A., Najjar, R. G., Friedrichs, M. A. M., Cai, W. J.,
678 Salisbury, J., Wang, Z. A., Thomas, H., and Shadwick, E.: Surface ocean *p*CO₂
679 seasonality and sea-air CO₂ flux estimates for the North American east coast,
680 Journal of Geophysical Research-Oceans, 118, 5439-5460, 10.1002/jgrc.20369,
681 2013.
- 682 Takahashi, T., Sutherland, S. C., Feely, R. A., and Wanninkhof, R.: Decadal change of
683 the surface water *p*CO₂ in the North Pacific: A synthesis of 35 years of
684 observations, Journal of Geophysical Research-Oceans, 111, Artn C07s05,
685 10.1029/2005jc003074, 2006.
- 686 Takahashi, T., Sutherland, S. C., Wanninkhof, R., Sweeney, C., Feely, R. A., Chipman,
687 D. W., Hales, B., Friederich, G., Chavez, F., Sabine, C., Watson, A., Bakker, D. C.
688 E., Schuster, U., Metzl, N., Yoshikawa-Inoue, H., Ishii, M., Midorikawa, T., Nojiri,
689 Y., Kortzinger, A., Steinhoff, T., Hoppema, M., Olafsson, J., Arnarson, T. S.,
690 Tilbrook, B., Johannessen, T., Olsen, A., Bellerby, R., Wong, C. S., Delille, B.,
691 Bates, N. R., and de Baar, H. J. W.: Climatological mean and decadal change in
692 surface ocean *p*CO₂, and net sea-air CO₂ flux over the global oceans, Deep-Sea
693 Research Part II-Topical Studies in Oceanography, 56, 554-577,
694 10.1016/j.dsr2.2008.12.009, 2009.
- 695 Telszewski, M., Chazottes, A., Schuster, U., Watson, A. J., Moulin, C., Bakker, D. C.
696 E., Gonzalez-Davila, M., Johannessen, T., Kortzinger, A., Luger, H., Olsen, A.,
697 Omar, A., Padin, X. A., Rios, A. F., Steinhoff, T., Santana-Casiano, M., Wallace, D.



- 698 W. R., and Wanninkhof, R.: Estimating the monthly $p\text{CO}_2$ distribution in the North
699 Atlantic using a self-organizing neural network, *Biogeosciences*, 6, 1405-1421,
700 DOI 10.5194/bg-6-1405-2009, 2009.
- 701 Wang, Y., Li, X., Song, J., Zhong, G., and Zhang, B.: Carbon Sinks and Variations of
702 $p\text{CO}_2$ in the Southern Ocean from 1998 to 2018 Based on a Deep Learning
703 Approach, *IEEE Journal of Selected Topics in Applied Earth Observations and*
704 *Remote Sensing*, 2021.
- 705 Wanninkhof, R., Park, G. H., Takahashi, T., Sweeney, C., Feely, R., Nojiri, Y., Gruber,
706 N., Doney, S. C., McKinley, G. A., Lenton, A., Le Quere, C., Heinze, C.,
707 Schwinger, J., Graven, H., and Khatiwala, S.: Global ocean carbon uptake:
708 magnitude, variability and trends, *Biogeosciences*, 10, 1983-2000, 10.5194/bg-10-
709 1983-2013, 2013.
- 710 Watson, A. J., Schuster, U., Shutler, J. D., Holding, T., Ashton, I. G. C.,
711 Landschuetzer, P., Woolf, D. K., and Goddijn-Murphy, L.: Revised estimates of
712 ocean-atmosphere CO_2 flux are consistent with ocean carbon inventory, *Nature*
713 *Communications*, 11, 10.1038/s41467-020-18203-3, 2020.
- 714 Weiss, R. F.: Carbon dioxide in water and seawater: the solubility of a non-ideal gas,
715 *Marine Chemistry*, 2, 203--215, 1974.
- 716 Zeng, J., Nojiri, Y., Landschützer, P., Telszewski, M., and Nakaoka, S.: A Global
717 Surface Ocean $f\text{CO}_2$ Climatology Based on a Feed-Forward Neural Network,
718 *Journal of Atmospheric and Oceanic Technology*, 31, 1838-1849, 10.1175/jtech-d-
719 13-00137.1, 2014.
- 720 Zeng, J. Y., Nojiri, Y., Nakaoka, S., Nakajima, H., and Shirai, T.: Surface ocean CO_2
721 in 1990-2011 modelled using a feed-forward neural network, *Geosci Data J*, 2, 47-
722 51, 10.1002/gdj3.26, 2015.
- 723 Zeng, J. Y., Matsunaga, T., Saigusa, N., Shirai, T., Nakaoka, S., and Tan, Z. H.:
724 Technical note: Evaluation of three machine learning models for surface ocean CO_2
725 mapping, *Ocean Sci*, 13, 303-313, 10.5194/os-13-303-2017, 2017.
- 726 Zhong, G., Li, X., Qu, B., Wang, Y., Yuan, H., and Song, J.: A General Regression
727 Neural Network approach to reconstruct global $1^\circ \times 1^\circ$ resolution sea surface $p\text{CO}_2$,
728 *Acta Oceanol Sin*, 10, 70-79, 10.3969/j.issn.0253-4193.2020.10.007, 2020.